Smart strategy to synthesis silver-based heterogeneous photocatalysts grown from molybdenum oxide precursor

Wei Wei[1,2] ✉, *Zhi Feng Jiang*[2,3], *Jun Jie Jing*[2], *Xiao Meng Lv*[2], *Ji Min Xie*[2]

[1]*Center of Analysis and Test, Jiangsu University, Zhenjiang, 212013, People's Republic of China*
[2]*School of Chemistry & Chemical Engineering, Jiangsu University, Zhenjiang, 212013, People's Republic of China*
[3]*School of Life Sciences, The Chinese University of Hong Kong, Hong Kong, 999077, People's Republic of China*
✉ *E-mail: weiwei@ujs.edu.cn*

Published in Micro & Nano Letters; Received on 14th March 2017; Revised on 10th June 2017; Accepted on 4th July 2017

Three silver-based photocatalysts, Ag@AgBr, $Ag_2Mo_2O_7$, and Ag_2MoO_4-MoO_3, were successfully synthesised by a smart hydrothermal strategy using molybdenum oxide as precursor in surfactant-assisted processes. The correlation among crystal structure and properties in the photocatalysts are discussed in detail. In addition to morphology control, the bromine source effect of adding surfactant cetyltrimethyl ammonium bromide in hydrothermal synthesis of plasmonic silver incorporated silver bromide photocatalyst was also found. The obtained Ag@AgBr showed higher photocatalytic activity in the degradation of methylene blue than other samples due to super sensitivity of AgBr to light and the surface plasmon resonance of Ag nanoparticles in the region of visible light.

1. Introduction: In recent years, silver-based heterogeneous photocatalysts have been widely studied for environment decontamination due to their potential applications in wastewater purifying [1, 2]. Generally, it is known that silver-based semiconductor can combine or react with other materials to produce a new enhanced photocatalytic activity catalyst, such as $AgBr/Ag_2CO_3$ [3], activated carbon/AgBr [4], Ag@AgBr [5], $Ag_2Mo_2O_7$@AgBr–Ag [6] and so on. They also have particular physical properties and good chemical stability, and are significantly active as catalysts for various organic pollution treatments.

For adsorption and photocatalytic properties of photocatalyst are closed related to their microstructure and morphology, many methods are morphology control in synthesis process by controlling experimental conditions [5, 7] or adding assistant additives [6, 8]. Nowadays, there are many researchers prepared the controllable nanostructured catalysts using special precursors [9–12]. It is usually believed that these precursors (MoO_3, SiO_2, WO_3 etc.) were only assisted in its function of morphology control in preparation process. Shen *et al.* [13] reported an in situ anion-exchange method for the preparation of $Ag@Ag_2MoO_4$–AgBr composite using Ag_2MoO_4 as precursors. Therefore, to clarify the current fuzzy perception of their functions in photocatalyst synthesis, the profoundly understood on the roles of precursors in the process would be investigated by systematical characterisation in this study.

Herein, MoO_3 rods were synthesised via are routine hydrothermal process. Afterwards, an in situ hydrothermal reaction between silver ion and cetyltrimethyl ammonium bromide (CTAB) was conducted to produce Ag@AgBr, $Ag_2Mo_2O_7$, and Ag_2MoO_4-MoO_3 under in various pH conditions. It was found that Ag@AgBr showed a much higher photocatalytic activity via degradation of methylene blue (MB) under visible light irradiation. The novel synthetic strategy presented here gives a promising route towards the development of stable plasmonic photocatalyst semiconductor.

2. Experimental: In advance, 5 mmol $(NH_4)_6Mo_7O_{24}\bullet 4H_2O$ was dissolved in water, then 4 mol/l HCl solution was added slowly into the above solution until the pH was 1.0. The suspension was poured into a autoclave and maintained at 140°C for 24 h. Then, the molybdenum oxide powder was collected by filtration, washed with water and ethanol, and finally dried at 80°C [12]. In a typical procedure, 6 mmol MoO_3 powder was put into 60 ml water under continuous stirring. After 15 min, 7 mmol ammonium fluoride (NH_4F), 1.5 mmol CTAB ($C_{16}H_{36}BrN$), and 6 mmol $AgNO_3$ were added to the suspension. Finally, the pH value of the solution was adjusted by using 4 mol/l HNO_3 and 6 mol/l ammonia solutions. The mixture was then transferred into a 50 ml Teflon-lined autoclave. The autoclave was maintained at 180°C for 12 h and naturally cooled down to room temperature. The solid precipitate were washed several times with distilled water and absolute ethanol, and then dried at 80°C for 12 h.

Characterisation: The structure and morphology of the products were characterised by a power X-ray diffraction (XRD) (Bruker AXS Company, Germany). The morphologies of the products were observed using scanning electron microscopy (SEM) (JEOL JSM-7001F, Japan). The chemical elements of the sample were determined by energy dispersive x-ray spectroscopy (EDX). X-ray photoelectron spectroscopy (XPS) analysis was measured on an ESCALAB MK X-ray photoelectron spectrometer. UV-vis diffuse reflectance spectra were characterised using a Shimadzu UV-2600 spectrophotometer.

Photocatalytic activity measurement: The photocatalytic activities of the products were assessed by degradation of MB solution under 300 W tungsten lamp equipped with a 420 nm cut-off filter. 40 mg photocatalyst was poured into 50 ml MB solution (10 mg/l) and stirred magnetically for 30 min in the dark to attain the absorption-desorption equilibrium of MB on the photocatalyst at room temperature. Based on the adsorption–desorption behaviour results of photocatalysts within 30 min in the dark, it could be believed that the adsorption–desorption behaviour had reached an equilibrium because of the slight change in the concentration of dye. The sample interval is 30 min. The concentrations of MB were tested with a UV-vis spectrophotometer in terms of the absorbance at 664 nm during the photodegradation process.

3. Results and discussion: The characteristic patterns of MoO_3 are shown in Fig. 1. These results show that the hexagonal phase MoO_3 macrorods (JCPDS Card No. 21-0569) were successfully synthesised [12]. The crystal structures of silver-based heterogeneous photocatalysts were determined by XRD. As shown in Fig. 2*a*, it can be seen that the sample synthesised at pH = 1 is indexed as Ag@AgBr with two additional peaks, which are indexed to the metal silver (JCPDS Card No. 65-2871) and pure AgBr

doi: 10.1049/mnl.2017.0152

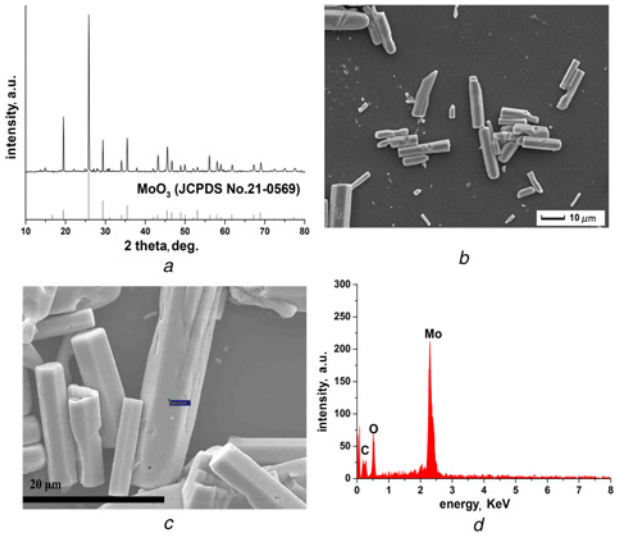

Fig. 1 *Characteristic patterns of MoO_3 macrorods*

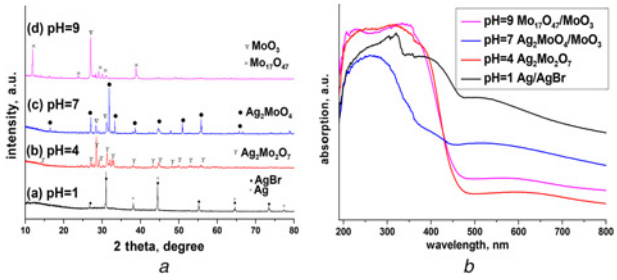

Fig. 2 *Sample synthesised at pH = 1 is indexed as Ag@AgBr with two additional peaks*
a XRD patterns of the silver-based heterogeneous photocatalysts
b UV-visible diffuse spectra of all as-prepared samples

(JCPDS Card No. 06-0438) [14]. Moreover, when the less acidic solution is used, the anorthic $Ag_2Mo_2O_7$ (JCPDS Card No. 75-1505) is obtained at pH 4 [15]. Meanwhile, a mixture of hexagonal MoO_3 and cubic Ag_2MoO_4 (JCPDS Card No. 75-250) was prepared at neutral environment [16]. However, the phases such as AgBr, $Ag_2Mo_2O_7$, and Ag_2MoO_4 are vanished in the samples obtained at alkaline condition. With pH increasing from 7 to 9, the finally product is found to be a mixture MoO_3 and $Mo_{17}O_{47}$ (JCPDS Card No. 13-0345). The UV-visible diffuse reflectance spectra of products are shown in Fig. 2*b*. The absorption edges of four samples extend to the visible-light region, the band gaps of the samples (Fig. 3) are estimated to be 2.42 eV for Ag@AgBr, and 2.63 eV for $Ag_2Mo_2O_7$, which is consistent with previous studies [6, 17]. The Ag@AgBr has a much stronger absorption in visible light area than others products, resulting from the surface plasmon resonance (SPR) of the Ag nanoparticles [14].

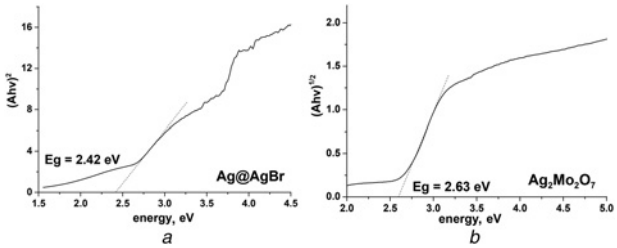

Fig. 3 *UV-vis diffuse reflectance of the samples*

The morphology and structure of as-synthesised products were characterised by the SEM, and the results were presented in Fig. 4. Fig. 4*a* shows the SEM image of the $Ag_2Mo_2O_7$, suggesting the existence of microrod structure. The rods are about 20–30 μm in length and 3–6 μm in diameter. Meanwhile, the polyhedron-like Ag_2MoO_4 and MoO_3 macrorods were shown in Fig. 4*b*. The shape of Ag_2MoO_4 is irregular while the MoO_3 is still macrorods. It can be seen that the length of MoO_3 macrorod is shorter than the MoO_3 precursor (Fig. 1). In Fig. 4*c* it be seen that the $Mo_{17}O_{47}$ nanoparticles attach on the MoO_3 macrorods to assemble composite. Typical SEM images Figs. 4*d* and *e* indicate that the Ag@AgBr is made up of sphere-like morphology with diameters of 1–3 μm. The inset is the high-magnification SEM image, in which it can be seen that the Ag nanoparticles are distributed uniformly on the surface of sphere-like AgBr. The result from EDX (Fig. 4*f*) shows that the products are composed of the elements of Ag and Br. The chemical state for the as-synthesised Ag@AgBr was further analysed by XPS. Fig. 5*a* shows the overview XPS spectra of Ag@AgBr, which exhibits the peaks of Ag, Br, and C. The sources of the peaks are $AgNO_3$ and CTAB, which is consistent with previously reported [8, 14]. Fig. 5*b* further shows that Ag is attached on the surface of AgBr, because the $Ag^0$3d peaks (367.5 and 373.6 eV) are in the Ag3d XPS spectra.

The possible formation mechanisms of products obtained in different pH are illustrated in Fig. 6. In the CTAB-assisted process, the surfactant molecule contains hydrophobic long chain belong to the positively charged group. When the cationic surfactant was dissolved in solution, the molecules can form monolayer structure tend to arrange into micelles during the hydrothermal process [13]. Since CTAB is a kind of strong-acid-weak-base salt, it can accelerate the ionisation process of MoO_4^{2-}. The formation mechanism could be divided into the four pH conditions, and the reaction process can be expressed as equations. The materials results from the different pH condition of MoO_4^{2-} and Ag^+ in the hydrothermal environment [12]. In pH = 1, the H^+ ions can enhance the dissolution and reaction of $Ag_2Mo_2O_7$ with Br^- by nucleophilic substitution [6], with the increase of hydrothermal reaction time, Ag@AgBr were obtained. In pH = 7, the redundant MoO_3 are still existed, when Ag_2MoO_4 product were formation in order to maintain element conservation. In pH = 9, the formation of silver ammino complex ion may lead the Ag^+ cannot reaction with other component, the final solid product is only MoO_3-$Mo_{17}O_{47}$ composite.

pH = 1 Ag@AgBr

$$2MoO_3 + 2F^- \rightarrow MoO_4^{2-} + MoO_2F_2 \quad (1)$$

$$MoO_2F_2 + 2H_2O \rightarrow MoO_4^{2-} + 2F^- + 4H^+ \quad (2)$$

$$2H^+ + 2Ag^+ + 2MoO_4^{2-} \rightarrow Ag_2Mo_2O_7 + H_2O \quad (3)$$

$$Ag_2Mo_2O_7 + 2Br^- \xrightarrow{H^+} 2AgBr + Mo_2O_7^{2-} \xrightarrow{H^+} Ag@AgBr \quad (4)$$

pH = 4 $Ag_2Mo_2O_7$

$$2MoO_3 + 2F^- \rightarrow MoO_4^{2-} + MoO_2F_2 \quad (5)$$

$$MoO_2F_2 + 2H_2O \rightarrow MoO_4^{2-} + 2F^- + 4H^+ \quad (6)$$

$$2H^+ + 2Ag^+ + 2MoO_4^{2-} \rightarrow Ag_2Mo_2O_7 + H_2O \quad (7)$$

pH = 7 Ag_2MoO_4- MoO_3

$$2MoO_3 + 2F^- \rightarrow MoO_4^{2-} + MoO_2F_2 \quad (8)$$

$$MoO_2F_2 + 2H_2O \rightarrow MoO_4^{2-} + 2F^- + 4H^+ \quad (9)$$

$$2Ag^+ + MoO_4^{2-} \rightarrow Ag_2MoO_4 \quad (10)$$

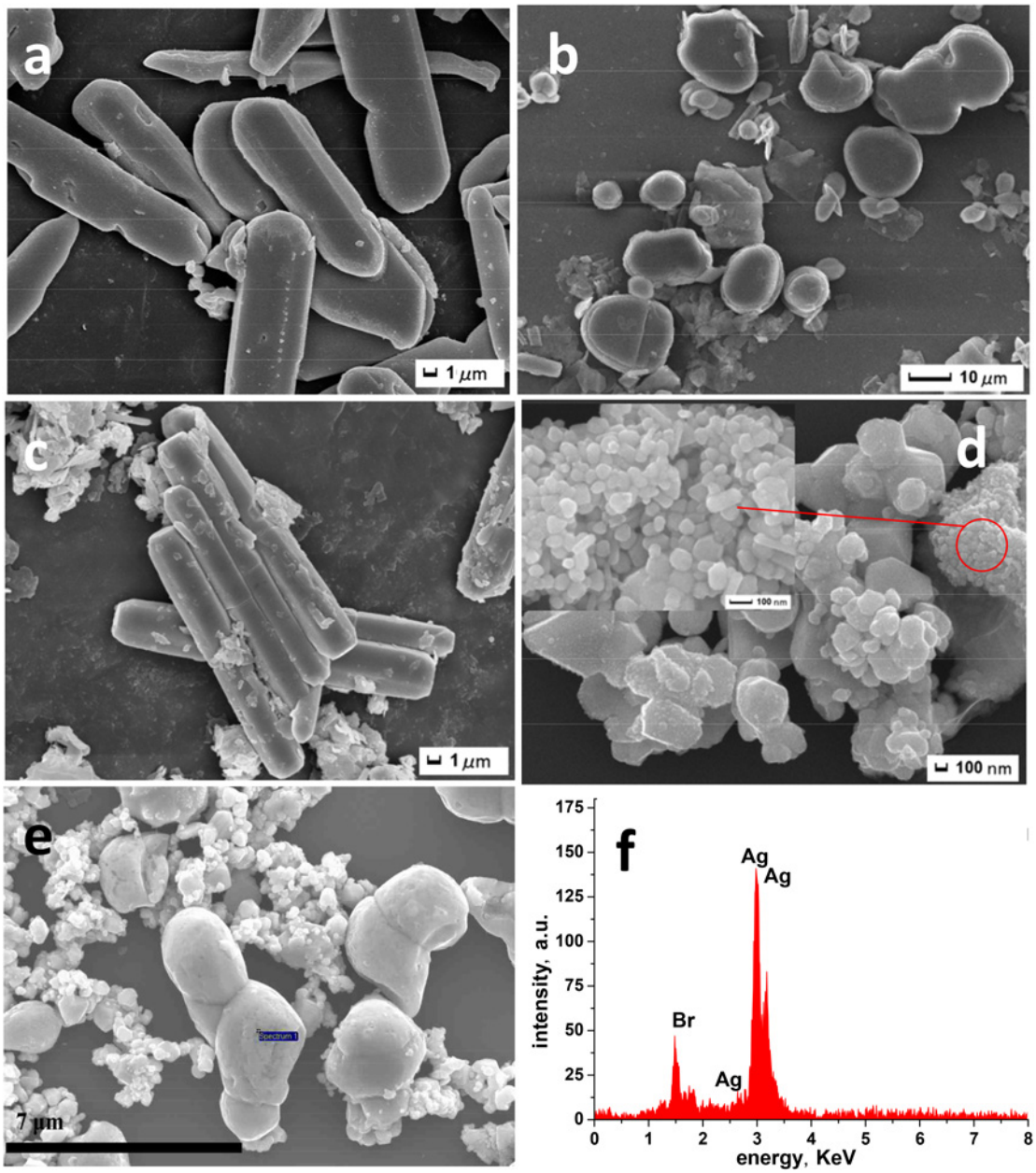

Fig. 4 *Morphology and structure of as-synthesised products were characterised by the SEM*
a SEM image of $Ag_2Mo_2O_7$ microrods
b SEM image of the polyhedron-like Ag_2MoO_4 with MoO_3 microrods
c SEM image of MoO_3-$Mo_{17}O_{47}$ composite
d, *e* SEM images of Ag@AgBr with different magnification
f EDX pattern of the Ag@AgBr sample

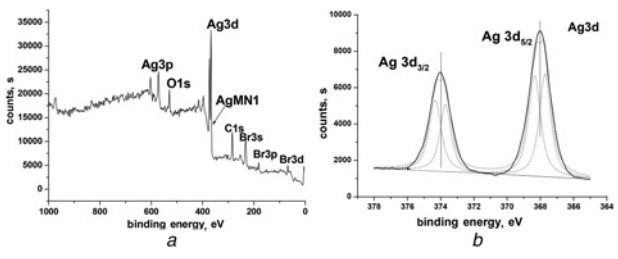

Fig. 5 *XPS spectrums of the as-prepared Ag@AgBr*
a Overview XPS spectra
b Ag3d XPS spectra

pH = 9 MoO_3-$Mo_{17}O_{47}$

$$2MoO_3 + 2F^- \rightarrow MoO_4^{2-} + MoO_2F_2 \quad (11)$$

$$34OH^- + 17MoO_2F_2 \rightarrow Mo_{17}O_{47} + 34F^- + 17H_2O \quad (12)$$

Fig. 7*a* indicates that Ag@AgBr exhibits excellent performance in the degradation of MB and the main absorbance peak of it almost disappears in 180 min. In Fig. 7*b*, a blank test confirmed that MB aqueous solution was stable to self-photolysis could be neglected. Meanwhile, Ag@AgBr exhibit excellent visible light photocatalytic activity that could degrade MB by 97.89%. To further clarify the reaction kinetics of MB degradation, the apparent pseudo-first-order model expressed by equation was applied in the experiments [18]: ln $(C_0/C) = k_{app}.t$ (k_{app} is the apparent pseudo-first-order rate

doi: 10.1049/mnl.2017.0152

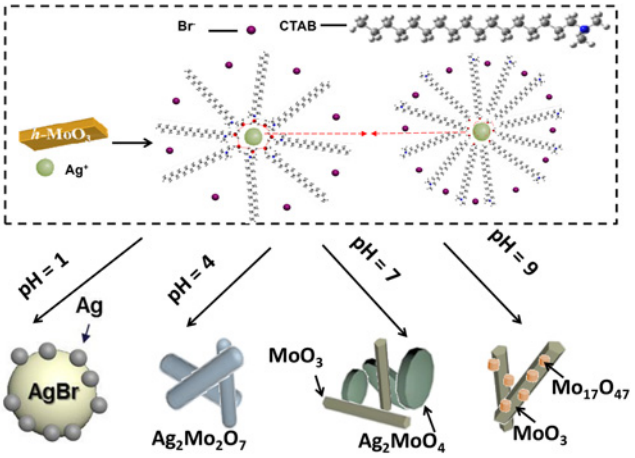

Fig. 6 *Schematic illustration of as-obtained samples with different pH*

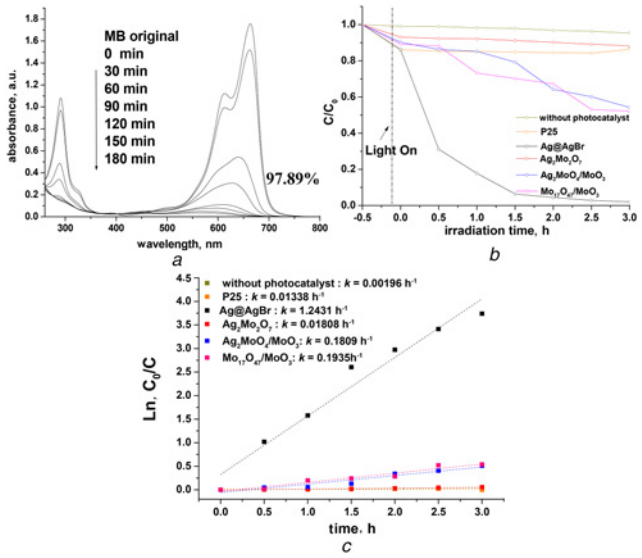

Fig. 7 *Ag@AgBr exhibits excellent performance in the degradation of MB and the main absorbance peak of it almost disappears in 180 min*
a UV-vis spectral changes of MB dye by Ag@AgBr
b Adsorption and photo-degradation of MB under visible-light irradiation by different samples
c Ln(C_0/C) –T for photocatalytic degradation of MB

constant, h^{-1}). The results (Fig. 4*c*) show that the catalytic activity is in the order Ag@AgBr > MoO_3-$Mo_{17}O_{47}$ > Ag_2MoO_4-MoO_3 > P25 > $Ag_2Mo_2O_7$. By comparison, it can be seen that the photocatalytic activity of Ag@AgBr was superior to that of other samples as a result of Ag nanoparticles SPR produced by the collective oscillation of surface electrons [14].

4. Conclusion: In summary, Ag@AgBr plasmonic photocatalyst was synthesised by a hydrothermal approach using *h*-MoO_3 macrorods as precursors with CTAB was employed as the morphology and bromine source controller. The experimental results indicated that Ag@AgBr show higher photocatalytic activity than other samples (MoO_3-$Mo_{17}O_{47}$, $Ag_2Mo_2O_7$, Ag_2MoO_4-MoO_3 by different pH condition) under visible light irradiation due to super sensitivity of AgBr to light and the SPR of Ag nanoparticles in the region of visible light. Moreover, the possible growth mechanism has been proposed.

5. Acknowledgments: This work was supported by the National Natural Science Foundation of China (grant no. 21607063), China Postdoctoral Science Foundation (grant no. 2016M590421) and Jiangsu Planned Projects for Postdoctoral Research Funds (grant no. 1501025A).

6 References

[1] Zhou X., Liu G., Yu J., *ET AL.*: 'Surface plasmon resonance-mediated photocatalysis by noble metal-based composites under visible light', *J Mater. Chem.*, 2012, **22**, (40), pp. 21337–21354
[2] Wen C., Yin A., Dai W.-L.: 'Recent advances in silver-based heterogeneous catalysts for green chemistry processes', *Appl. Catal. B-Environ.*, 2014, **160-161**, pp. 730–741
[3] Xie J., Fang C., Zou J., *ET AL.*: 'In situ ultrasonic formation of AgBr/Ag_2CO_3 nanosheets composite with enhanced visible-driven photocatalytic performance', *Mater. Lett.*, 2016, **170**, pp. 62–66
[4] Wang D., Zhao M., Luo Q., *ET AL.*: 'An efficient visible-light photocatalyst prepared by modifying AgBr particles with a small amount of activated carbon', *Mater. Res. Bull.*, 2016, **76**, pp. 402–410
[5] Xiao X., Ge L., Han C., *ET AL.*: 'A facile way to synthesize Ag@Agbr cubic cages with efficient visible-light-induced photocatalytic activity', *Appl. Catal. B-Environ.*, 2015, **163**, pp. 564–572
[6] Shen C.-C., Zhu Q., Zhao Z.-W., *ET AL.*: 'Plasmon enhanced visible light photocatalytic activity of ternary $Ag_2Mo_2O_7$@AgBr–Ag rod-like heterostructures', *J. Mater. Chem. A*, 2015, **3**, (28), pp. 14661–14668
[7] Cheng Z., Chu X., Sheng Z., *ET AL.*: 'Synthesis of quasi-spherical Agbr microcrystal via a simple ion-exchange route', *Mater. Lett.*, 2016, **168**, pp. 99–102
[8] Bai Y.Y., Lu Y., Liu J.K.: 'An efficient photocatalyst for degradation of various organic dyes: Ag@Ag_2MoO_4-AgBr composite', *J Hazard. Mater.*, 2016, **307**, pp. 26–35
[9] Wang D., Duan Y., Luo Q., *ET AL.*: 'Visible light photocatalytic activities of plasmonic Ag/AgBr particles synthesized by a double jet method', *Desalination*, 2011, **270**, (1-3), pp. 174–180
[10] Chen Y., Tian G., Shi Y., *ET AL.*: 'Hierarchical MoS_2/Bi_2MoO_6 composites with synergistic effect for enhanced visible photocatalytic activity', *Appl. Catal. B-Environ.*, 2015, **164**, pp. 40–47
[11] Li G., Li C., Tang H., *ET AL.*: 'Synthesis and characterization of hollow MoS_2 microspheres grown from MoO_3 precursors', *J Alloy. Compd.*, 2010, **501**, (2), pp. 275–281
[12] Shang M., Wang W., Ren J., *ET AL.*: 'Nanoscale kirkendall effect for the synthesis of Bi 2 Moo 6 boxes via a facile solution-phase method', *Nanoscale*, 2011, **3**, (4), pp. 1474–1476
[13] Wei W., Gao J., Jiang Z., *ET AL.*: 'Transforming MoO_3 macrorods into bismuth molybdate nanoplates via the surfactant-assisted hydrothermal method', *Ceram. Int.*, 2015, **41**, (9), pp. 11471–11481
[14] Kuai L., Geng B., Chen X., *ET AL.*: 'Facile subsequently light-induced route to highly efficient and stable sunlight-driven Ag@AgBr plasmonic photocatalyst', *Langmuir*, 2010, **26**, (24), pp. 18723–18727
[15] Cui X., Yu S.H., Li L., *ET AL.*: 'Selective synthesis and characterization of single crystal silver molybdate/tungstate nanowires by a hydrothermal process', *Chem.-Eur. J.*, 2004, **10**, (1), pp. 218–223
[16] Wang P., Huang B., Lou Z., *ET AL.*: 'Synthesis of highly efficient Ag@AgCl plasmonic photocatalysts with various structures', *Chem.-Eur. J.*, 2010, **16**, (2), pp. 538–544
[17] Yan X., Wang X., Gu W., *ET AL.*: 'Single-crystalline $AgIn(MoO_4)_2$ nanosheets grafted Ag/AgBr composites with enhanced plasmonic photocatalytic activity for degradation of tetracycline under visible light', *Appl. Catal. B-Environ.*, 2015, **164**, pp. 297–304
[18] Cao J., Xu B., Lin H., *ET AL.*: 'Chemical etching preparation of BiOI/BiOBr heterostructures with enhanced photocatalytic properties for organic dye removal', *Chem. Eng. J*, 2012, **185**, pp. 91–99